

Numerical Method of Characteristics for One-Dimensional Blood Flow

Sebastián Acosta¹, Charles Puelz², Béatrice Rivière², Daniel J. Penny¹, Craig G. Rusin¹

Abstract

Mathematical modeling at the level of the full cardiovascular system requires the numerical approximation of solutions to a one-dimensional nonlinear hyperbolic system describing flow in a single vessel. This model is often simulated by computationally intensive methods like finite elements and discontinuous Galerkin, while some recent applications require more efficient approaches (e.g. for real-time clinical decision support, phenomena occurring over multiple cardiac cycles, iterative solutions to optimization/inverse problems, and uncertainty quantification). Further, the high speed of pressure waves in blood vessels greatly restricts the time-step needed for stability in explicit schemes. We address both cost and stability by presenting an efficient and unconditionally stable method for approximating solutions to diagonal nonlinear hyperbolic systems. Theoretical analysis of the algorithm is given along with a comparison of our method to a discontinuous Galerkin implementation. Lastly, we demonstrate the utility of the proposed method by implementing it on an arterial network of 64 vessels whose elastic and geometrical parameters are physiologically relevant.

Key words: Blood flow, computational hemodynamics, characteristics, wave propagation.

1. Introduction

Recent research on hemodynamic models utilize a set of equations describing blood flow in a single vessel. In this model, the variables of interest are the vessel cross-sectional area $A = A(x, t)$ and the average blood velocity in the axial direction x given as $u = u(x, t)$. Conservation of mass and balance of momentum result in the following system of equations:

$$\begin{aligned} \frac{\partial A}{\partial t} + \frac{\partial(Au)}{\partial x} &= 0 \\ \frac{\partial u}{\partial t} + \frac{\partial}{\partial x} \left(\frac{u^2}{2} + \frac{p}{\rho} \right) &= -\mu \frac{u}{A}. \end{aligned} \tag{1}$$

We call (1) the (A, u) system. Here $\rho = 1.06 \text{ g/cm}^3$ is the density of blood and $\mu = 3.5 \text{ cP}$ is its dynamic viscosity. The assumptions of this model include the following: blood is an incompressible, viscous fluid flowing in a straight cylinder with compliant walls, the characteristic length of

¹Baylor College of Medicine, Department of Pediatric Cardiology

²Rice University, Department of Computational and Applied Mathematics

the vessel (along the axial direction) is much larger than the characteristic radius, and the velocity profile is flat. For further details and a discussion of the related $(A, Q := Au)$ model, see for example the works of Canic et al., Formaggia et al. and Sherwin et al. [1, 2, 3, 4]. We choose to work with the (A, u) system since our discontinuous Galerkin formulation is based on the work of Sherwin et al., but our method may be applied to other related models of 1d blood flow [4].

To close the system, the functional relationship for the pressure p is provided by the state equation

$$p = p_{\text{ext}} + \beta(A^{1/2} - A_0^{1/2}) \quad (2)$$

where p_{ext} is the external pressure and A_0 is the vessel cross-sectional area for vanishing transmural pressure difference. The coefficient β is known as the elastic constant of the vessel wall.

These equations appear in recent literature for simulations of blood flow in a network of connected vessels, where system (1) models flow in each vessel and appropriate transmission conditions between vessels are specified. As an example, vessel-network models of the full cardiovascular system provide important insight into different clinical and physiological questions. Clinicians and engineers interested in the fluid dynamics around the heart may couple a 2d or 3d model of fluid flow close to the heart to a 1d network model of the arterial tree (and perhaps the venous tree). This modeling approach has at least two benefits: first, the high fidelity 1d model of the arterial tree replaces overly simplistic lumped parameter models, and second, one may interrogate the 1d arterial tree model to better understand fluid flow in the peripheral circulation and the reflection of pressure waves. For some examples of 1d models derived from system (1) or the (A, Q) system coupled to higher dimensional models see [5, 6, 7]. Other clinical applications include stent flow simulations, models of fetus and neonate circulations, and surgical planning [3, 8, 9, 4]. This collection of references, although not comprehensive, is meant to emphasize the versatility of (1).

Finite element, finite volume, discontinuous Galerkin, and other methods arising from weak formulations are successfully used for the spatial discretization of the (A, u) or (A, Q) systems [10, 11, 4]. Although these methods maintain attractive mathematical properties, they are computationally intensive, and this complexity is magnified in simulations of vessel networks. For instance, the speed of pressure waves in blood vessels dictates the time-step required for stability in explicit schemes. Unfortunately, for physiologically relevant choices of parameters, this speed may be much larger (at least one order of magnitude) than the velocity of blood flow. Moreover, the speed of pressure waves in the arterial tree generally increases as the vessel radius decreases. This implies that the inclusion of smaller arteries in the model (to obtain more realistic and accurate simulations) results in a more stringent stability condition. For a side-by-side comparison of several methods, see the recent paper by Wang et al. [12]. These authors compare methods for simulating (1) based on several metrics, including running time for one cardiac cycle.

In some instances, a more expensive discretization from a weak formulation is appropriate. But for our applications, we envision a 1d vessel-network model as a component in clinical decision support systems requiring simulation of multiple cardiac cycles. Fast iterative or repeated simulations are also needed for uncertainty quantification or to solve inverse problems via optimization. In these cases, close to real-time simulation is essential, and as such, the method for approximating solutions to (1) must be efficient and unconditionally stable. Fortunately, system (1) is strictly hyperbolic and has explicitly defined characteristic variables, allowing the use of a

numerical method of characteristics (NMC) for solving these equations. The method we propose is explicit in time (which makes it computational efficient) and unconditionally stable since no CFL-type condition is required to maintain stability.

Many methods for numerically solving differential equations based on the characteristics have been proposed in the past. Some address the transport of a certain solvent or convection-dominated diffusion equations [13, 14, 15, 16, 17, 18, 19]. Other works deal with approximations for Navier-Stokes equations in the absence of fluid-structure interaction [20, 21, 22] where the convective-derivative of the fluid velocity is treated with the method of characteristics. The concept behind the numerical method of characteristics also constitutes a main ingredient in the CIP method developed in [23, 24, 25, 26]. Furthermore, variants of this method have very recently been applied in the hemodynamics context [27, 28, 29]. Unfortunately, these latter publications do not rigorously address stability and convergence.

This manuscript details the application of the NMC method to blood flow (Sections 2-3) and develops the standard numerical analysis (Section 4). Our analysis is supported with numerical experiments to confirm the proven rate of convergence and to compared the NMC method with a discontinuous Galerkin (dG) discretization of (1). We conclude with an application of the NMC method to an arterial network of vessels (Section 5).

2. Characteristics for one-dimensional blood flow

In this section, we recapitulate some useful mathematical properties of (1). First, let us consider a general system of the form:

$$\frac{\partial \mathbf{U}}{\partial t} + \frac{\partial \mathbf{F}(\mathbf{U})}{\partial x} = \mathbf{S}(\mathbf{U}) \quad (3)$$

where $\mathbf{U} \in \mathbb{R}^2$ ($\mathbf{U} = (u_1, u_2)^T$). This system may be written in a quasilinear form, namely

$$\frac{\partial \mathbf{U}}{\partial t} + \nabla_{\mathbf{U}} \mathbf{F} \frac{\partial \mathbf{U}}{\partial x} = \mathbf{S}(\mathbf{U}) \quad (4)$$

where $\nabla_{\mathbf{U}} \mathbf{F}$ is the 2×2 Jacobian matrix of \mathbf{F} and the source function may change to include some terms from differentiating \mathbf{F} . As we shall see, (1) may be expressed in this form. Let the left eigenvectors of $\nabla_{\mathbf{U}} \mathbf{F}$ be given as $\{\mathbf{l}_1(\mathbf{U}), \mathbf{l}_2(\mathbf{U})\}$ with eigenvalues $\{\lambda_1(\mathbf{U}), \lambda_2(\mathbf{U})\}$ (we will henceforth drop the notation indicating their dependence on \mathbf{U}). The system (3) is *strictly hyperbolic* provided the Jacobian matrix has real distinct eigenvalues.

The general idea for the method of characteristics is to transform system (3) by diagonalizing the principal part of the differential equation in the hope that one finds functions remaining constant along particular curves. With this in mind, consider $Z_i : \mathbb{R}^2 \rightarrow \mathbb{R}$ whose gradient $\nabla_{\mathbf{U}} Z_i := \left(\frac{\partial Z_i}{\partial u_1}, \frac{\partial Z_i}{\partial u_2} \right)^T$ is parallel to \mathbf{l}_i ; these are called *Riemann-invariants* (see e.g. [30, pp. 637]). Now, define functions V_1 and V_2 from Z_1 and Z_2 like

$$V_1(x, t) = Z_1(\mathbf{U}(x, t)) \quad (5)$$

$$V_2(x, t) = Z_2(\mathbf{U}(x, t)). \quad (6)$$

We refer to V_1 and V_2 as the *characteristics variables* of system (3). From the chain rule combined with (4), V_1 and V_2 satisfy

$$\frac{\partial V_1}{\partial t} + \lambda_1 \frac{\partial V_1}{\partial x} = \nabla_{\mathbf{U}} Z_1^T \mathbf{S}(\mathbf{U}) \quad (7)$$

$$\frac{\partial V_2}{\partial t} + \lambda_2 \frac{\partial V_2}{\partial x} = \nabla_{\mathbf{U}} Z_2^T \mathbf{S}(\mathbf{U}). \quad (8)$$

The next statement is important for our method. It is easy to see that the following holds.

Proposition 1. *The function $V_i(x, t) - \int_0^t \nabla_{\mathbf{U}} Z_i(\mathbf{U}(x, s))^T \mathbf{S}(\mathbf{U}(x, s)) ds$ is constant along the curve $(\gamma_i(s), s)$ satisfying*

$$\frac{d\gamma_i}{ds} = \lambda_i(\mathbf{U}(\gamma_i(s), s)).$$

We derive the characteristic variables for system (1) by following equations (5) – (8) with Proposition 1. First, we rewrite the system with the Jacobian of \mathbf{F} as follows (note that we assume β and A_0 to vary as functions of x and absorb these terms into the source function):

$$\underbrace{\frac{\partial}{\partial t} \begin{bmatrix} A \\ u \end{bmatrix}}_{\partial \mathbf{U} / \partial t} + \underbrace{\begin{bmatrix} u & A \\ \frac{1}{\rho} \frac{\partial p}{\partial A} & u \end{bmatrix}}_{\nabla_{\mathbf{U}} \mathbf{F}} \underbrace{\frac{\partial}{\partial x} \begin{bmatrix} A \\ u \end{bmatrix}}_{\partial \mathbf{U} / \partial x} = \underbrace{\frac{1}{\rho} \begin{bmatrix} 0 \\ -\mu_A^u - \frac{\partial p}{\partial \beta} \frac{d\beta}{dx} - \frac{\partial p}{\partial A_0} \frac{dA_0}{dx} \end{bmatrix}}_{\mathbf{S}(\mathbf{U})}.$$

Let

$$c = c(A) = \left(\frac{\beta \sqrt{A}}{2\rho} \right)^{1/2}.$$

The left eigenvectors and eigenvalues for $\nabla_{\mathbf{U}} \mathbf{F}$ are

$$\lambda_1 = u + c, \quad \mathbf{l}_1 = \begin{bmatrix} c/A \\ 1 \end{bmatrix}, \quad (9)$$

$$\lambda_2 = u - c, \quad \mathbf{l}_2 = \begin{bmatrix} -c/A \\ 1 \end{bmatrix}. \quad (10)$$

If we set $\nabla_{\mathbf{U}} Z_i = \mathbf{l}_i$ then with $\mathbf{U} = (A, u)^T$ we have

$$\begin{aligned} \frac{\partial Z_1}{\partial A} &= \frac{c}{A}, & \frac{\partial Z_1}{\partial u} &= 1, \\ \frac{\partial Z_2}{\partial A} &= -\frac{c}{A}, & \frac{\partial Z_2}{\partial u} &= 1. \end{aligned}$$

Integrating, we obtain:

$$V_1(x, t) = u(x, t) + 4c(A(x, t)) \quad (11)$$

$$V_2(x, t) = u(x, t) - 4c(A(x, t)), \quad (12)$$

where these variables satisfy the system

$$\begin{aligned}\frac{\partial V_1}{\partial t} + (u + c)\frac{\partial V_1}{\partial x} &= \hat{S}_1(V_1, V_2) \\ \frac{\partial V_2}{\partial t} + (u - c)\frac{\partial V_2}{\partial x} &= \hat{S}_2(V_1, V_2).\end{aligned}\tag{13}$$

and $\hat{S}_i := \nabla_{\mathbf{V}} Z_i^T \mathbf{S}$. One may recover the cross-sectional area (and hence the pressure from (2)) and velocity from the characteristic variables, and vice versa.

The above derivation reveals that the characteristic variables propagate at speeds $u \pm c$, where u is the speed of blood and for physiologically relevant parameter values, $c \gg |u|$. In particular, this relationship between u and c implies that $\lambda_1 > 0$ and $\lambda_2 < 0$.

Explicit time discretizations require a CFL-type restriction on the timestep determined by c despite the fact that the speed of blood u is much smaller. To avoid this strong restriction, we propose a method that is stable regardless of the chosen timestep.

3. Algorithm

For the presentation of the algorithm, let us focus on a system of two equations in the domain $[a, b]$ and the following initial conditions:

$$\frac{\partial V_1}{\partial t} + \lambda_1(x, t)\frac{\partial V_1}{\partial x} = 0 \tag{14}$$

$$\frac{\partial V_2}{\partial t} + \lambda_2(x, t)\frac{\partial V_2}{\partial x} = 0 \tag{15}$$

$$V_1(x, 0) = V_1^0(x) \tag{16}$$

$$V_2(x, 0) = V_2^0(x) \tag{17}$$

augmented by appropriate boundary conditions. We assume for the time interval of interest, say $[0, T]$, $\lambda_1 > 0$ and $\lambda_2 < 0$. Our analysis applies to systems with no source term and periodic boundary conditions, namely

$$V_i(a, t) = V_i(b, t) \text{ for } i = 1, 2. \tag{18}$$

The extension to equations with zeroth order terms (dissipation) or actual sources is accomplished following the same framework of the method of characteristics. In fact, Proposition 1 indicates that we ought to integrate the source term along the characteristic curve to correctly incorporate its influence on the solution. This can be done with numerical quadrature once the characteristic curve has been approximated successfully, which is the subject of this section.

First we introduce some notation. We use the following supremum norms in our analysis.

$$\|q\| := \sup_{x \in [a, b]} |q(x)| \tag{19}$$

Consider some final time $T > 0$. We define the norm over space and time as:

$$\|p\|_T := \sup_{x \in [a, b] \text{ and } t \in [0, T]} |p(x, t)|. \tag{20}$$

Let dashes denote derivatives in space and dots denote derivatives in time, i.e. $p' := \partial p / \partial x$ and $\dot{p} := \partial p / \partial t$. For the spatial discretization, let

$$G_h := \left\{ x_j = a + \frac{j(b-a)}{M}, j = 0, \dots, M \right\}, \quad (21)$$

i.e. the collection of uniformly spaced points between a and b with spacing $h := (b-a)/M$. Define $C[a, b]$ to be the space of continuous functions on $[a, b]$, and $C_h[a, b]$ to be the subset of continuous functions that are linear when restricted to each interval $[x_j, x_{j+1}]$ for $j = 0, \dots, M-1$.

For the temporal discretization, given a positive integer N , define the timestep $\Delta t := T/N$ and $t_n := n\Delta t$. To declutter notation, define

$$p^n(x) := p(x, t_n). \quad (22)$$

In what follows, V_i refers to the exact solution whereas W_i refers to the approximate solution.

To motivate the algorithm, observe that the function V_i ($i = 1, 2$) is constant in time along the *characteristic curve* γ_i defined by

$$\dot{\gamma}_i(t) = \lambda_i(\gamma_i(t), t). \quad (23)$$

One may obtain the value of V_i at any given time, given some initial condition $V_i(x, 0) = V_i^0(x)$, by shifting V_i^0 along the curve γ_i . The numerical method of characteristics for solving (14) – (17) is based on this idea: to obtain an approximation W_i to V_i given information on the grid G_h , follow the movement of the points in G_h along the characteristic curves *back* in time, and then assign values at the *current* time via spatial interpolation of the solution. More explicitly, from (23) the following equality holds:

$$\gamma_i(t + \Delta t) - \gamma_i(t) = \int_t^{t+\Delta t} \lambda_i(\gamma_i(s), s) ds. \quad (24)$$

Hence with $\gamma_i(t + \Delta t) = x \in G_h$, one has

$$V_i(x, t + \Delta t) = V_i(\gamma_i(t), t) = V_i\left(x - \int_t^{t+\Delta t} \lambda_i(\gamma_i(s), s) ds, t\right). \quad (25)$$

With this in mind, we have the following set of definitions. In light of (23), for each $x \in [a, b]$ define the characteristic curve $\gamma_i(x, t_{n+1}; t) : [t_n, t_{n+1}] \rightarrow \mathbb{R}$ passing through point x at time t_{n+1} as the solution to the following *final* value problem:

$$\frac{d\gamma_i(x, t_{n+1}; t)}{dt} = \lambda_i(\gamma_i(x, t_{n+1}; t), t) \quad (26)$$

$$\gamma_i(x, t_{n+1}; t_{n+1}) = x. \quad (27)$$

Definition 1. Let $n = 1, 2, \dots, N$. For $x \in [a, b]$, let $\tilde{g}_i^n(x)$ ($i = 1, 2$) be an approximation to the quantity

$$g_i^n(x) = x - \mathcal{I}_i^n(x) := x - \int_{t_n}^{t_{n+1}} \lambda_i(\gamma_i(x, t_{n+1}; t), t) dt \quad (28)$$

in the sense that

$$\tilde{g}_i^n(x) := x - \tilde{Q}_i^n(x) \quad (29)$$

where \tilde{Q}_i^n is a “pseudo–quadrature rule” for the integral I_i^n computed with the approximate solution W_i . Define Q_i^n to be this same pseudo–quadrature rule computed with the exact solution V_i . As we will see below, the rule we define is equivalent to a linearization of the characteristic curve. An illustration of the definition of $g^n(x)$ and $\tilde{g}^n(x)$ is displayed in Figure 1.

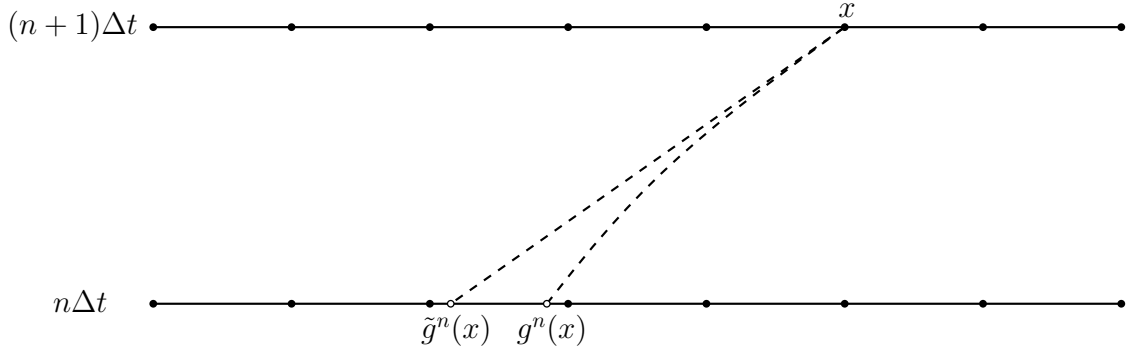


Figure 1: The characteristic curve and its approximation. The *head* of the characteristic curve is the grid point x , and its *foot* is denoted by $g^n(x)$. The approximate *foot*, denoted by $\tilde{g}^n(x)$, is obtained by a linearization of the characteristic curve given in Definition 1.

Remark 1. Note that $g_i^n(x)$ and $\tilde{g}_i^n(x)$ may not lie in the interval $[a, b]$, but its definition can be easily adjusted to handle the periodic boundary condition or a prescribed Dirichlet condition.

Take $x \in [a, b]$ and consider the characteristic curve within the time interval $[t_n, t_{n+1}]$ on which x lies at time t_{n+1} , i.e. $\gamma_i(x, t_{n+1}, t)$. By Definition 1 and (24) we have $g_i^n(x) = \gamma_i(x, t_{n+1}; t_n)$. In turn, for the solution V_i one has

$$\begin{aligned} V_i^{n+1}(x) &= V_i(x, t_{n+1}) \\ &= V_i(\gamma_i(x, t_{n+1}; t_{n+1}), t_{n+1}) \\ &= V_i(\gamma_i(x, t_{n+1}; t_n), t_n) \\ &= V_i(g_i^n(x), t_n) = V_i^n(g_i^n(x)). \end{aligned}$$

We have shown the following lemma which is nothing more than rewriting (25) in more compact notation.

Lemma 1. The solutions V_i to (14) – (17) satisfy

$$V_i^{n+1}(x) = V_i^n(g_i^n(x)) \quad \text{for all } x \in [a, b] \text{ and } n = 1 \dots N. \quad (30)$$

To define the quadrature rule \mathcal{Q}_i^n (and hence $\tilde{\mathcal{Q}}_i^n$), we view $\lambda_i(x, t)$ as a function of the characteristic variables $V_1(x, t)$ and $V_2(x, t)$. For example, for the blood flow system (1), one has,

$$\lambda_1(x, t) := \phi_1(V_1, V_2) = \frac{3}{4}V_1 + \frac{1}{4}V_2 \quad (31)$$

$$\lambda_2(x, t) := \phi_2(V_1, V_2) = \frac{1}{4}V_1 + \frac{3}{4}V_2, \quad (32)$$

so in accordance with our previous notation, we can write $\lambda_i(x, t_n) = \phi_i(V_1^n(x), V_2^n(x))$. In turn, we would like to approximate the integral by the simplest “rectangle rule”, i.e.

$$\mathcal{I}_i^n(x) \approx \Delta t \lambda_i(\gamma_i(x, t_{n+1}; t_n), t_n) = \Delta t \phi_i(V_1^n(g_i^n(x)), V_2^n(g_i^n(x))). \quad (33)$$

Let us define $\mathcal{Q}_{i,R}$ and $\tilde{\mathcal{Q}}_{i,R}$ via the rectangle rule approximation:

$$\mathcal{Q}_{i,R}^n(x) := \Delta t \phi_i(V_1^n(g_i^n(x)), V_2^n(g_i^n(x))) \quad (34)$$

$$\tilde{\mathcal{Q}}_{i,R}^n(x) := \Delta t \phi_i(W_1^n(\tilde{g}_i^n(x)), W_2^n(\tilde{g}_i^n(x))), \quad (35)$$

where $\tilde{\mathcal{Q}}_{i,R}^n$ is computed with the approximate solution W_1^n, W_2^n . If we were to take our pseudo-quadrature rule to be $\mathcal{Q}_i^n = \mathcal{Q}_{i,R}^n$ and $\tilde{\mathcal{Q}}_i^n = \tilde{\mathcal{Q}}_{i,R}^n$, then the formula to determine $\tilde{g}_i^n(x)$ becomes nonlinear and hence *implicit* in time ³, i.e.

$$\tilde{g}_i^n(x) = x - \Delta t \phi_i(W_1^n(\tilde{g}_i^n(x)), W_2^n(\tilde{g}_i^n(x))) := \mathcal{K}_i^n(\tilde{g}_i^n(x)). \quad (36)$$

To simplify the method and have an explicit time stepping procedure, we define the rule we implement from the rectangle rule by replacing both $g_i^n(x)$ and $\tilde{g}_i^n(x)$ with x in both $\mathcal{Q}_{i,R}^n$ and $\tilde{\mathcal{Q}}_{i,R}^n$ respectively. Explicitly, we have the following definition:

Definition 2. *The pseudo-quadrature rule is defined as follows:*

$$\mathcal{Q}_i^n(x) := \Delta t \phi_i(V_1^n(x), V_2^n(x)) \quad (37)$$

$$\tilde{\mathcal{Q}}_i^n(x) := \Delta t \phi_i(W_1^n(x), W_2^n(x)). \quad (38)$$

The last missing piece is the specification of the spatial interpolation procedure.

Definition 3. $\Pi_h : C[a, b] \rightarrow C_h[a, b]$ projects a continuous function f into its piecewise linear interpolant $\Pi_h f$ at the points in G_h .

With this notation, Algorithm 1 defines the numerical method of characteristics (NMC) in precise terms.

³For small enough Δt , \mathcal{K}^n is a contraction. If the rectangle rule scheme is employed, $\tilde{g}_i^n(x)$ may be computed as the limit of the sequence $y^{(k+1)} = \mathcal{K}^n(y^{(k)})$ with initial condition $y^{(0)} = x$.

Algorithm 1 NMC algorithm

- 1: **Input:** $V_1^0, V_2^0 \in C[a, b]$.
 - 2: Initialize $W_1^0 = \Pi_h[V_1^0]$ and $W_2^0 = \Pi_h[V_2^0]$.
 - 3: **for** $n = 1, 2, \dots, N$
 - 4: $\tilde{g}_1^{n-1}(x) = x - \Delta t \phi_1(W_1^{n-1}(x), W_2^{n-1}(x))$
 - 5: $\tilde{g}_2^{n-1}(x) = x - \Delta t \phi_2(W_1^{n-1}(x), W_2^{n-1}(x))$
 - 6: $W_1^n(x) = \Pi_h[W_1^{n-1}(\tilde{g}_1^{n-1}(x))]$
 - 7: $W_2^n(x) = \Pi_h[W_2^{n-1}(\tilde{g}_2^{n-1}(x))]$
 - 8: **end**
-

Remark 2. Higher order interpolation and quadrature is possible. We work with piecewise linear interpolation for our analysis since the norm of Π_h is uniformly bounded by 1 for all h which leads to stability. Also, the rule defined in Definition 2 allows our method to remain explicit in time.

Remark 3. In practice, we compute the approximate solution W_i at the points in G_h , but in the presentation of the algorithm above, the approximate solution is viewed equivalently as a piecewise linear function in $C_h[a, b]$. We use this presentation since we work with the continuous supremum norm for our analysis.

4. Numerical Analysis

Let $V_1(x, t)$, $V_2(x, t)$ and $W_1^n(x)$, $W_2^n(x)$ be the exact and approximate solutions to (14) – (17) respectively. We make the following assumptions:

Assumption 1. The exact solutions satisfy $V_i \in C^2([0, T] \times [a, b])$.

Assumption 2. The functions λ_i , as functions of the characteristic variables V_i , are Lipschitz continuous with constants $C_{i,\lambda}$. Explicitly,

$$|\phi_i(V_1, V_2) - \phi_i(\hat{V}_1, \hat{V}_2)| \leq C_{i,\lambda}(|V_1 - \hat{V}_1| + |V_2 - \hat{V}_2|), \quad i = 1, 2. \quad (39)$$

Further, $\lambda_i \in C^1([0, T] \times [a, b])$.

Note that Assumption 2 holds for system (1) since from (31), the eigenvalues λ_i are affine functions of the characteristic variables. We first prove stability of the algorithm, independent of the chosen timestep Δt .

Proposition 2 (Stability). The approximate solutions W_1^n , W_2^n satisfy:

$$\|W_1^n\| + \|W_2^n\| \leq \|W_1^0\| + \|W_2^0\|, \quad \text{for all } n = 1 \dots N.$$

Proof. This follows immediately using the fact that for piecewise linear interpolation we have $\|\Pi_h\| = 1$.

$$\begin{aligned} \|W_1^n\| + \|W_2^n\| &= \|\Pi_h[W_1^{n-1}(\tilde{g}_1^{n-1})]\| + \|\Pi_h[W_2^{n-1}(\tilde{g}_2^{n-1})]\| \\ &\leq \|\Pi_h\| \|W_1^{n-1}\| + \|\Pi_h\| \|W_2^{n-1}\| \\ &\leq \|W_1^{n-1}\| + \|W_2^{n-1}\|. \end{aligned}$$

□

A convergence result for the algorithm follows below.

Theorem 1 (Convergence). *Fix $T > 0$ and $\Delta t = T/N$ for $N \in \mathbb{N}$. Let C_* be a constant depending on $C_{\lambda,i}$ and bounds on the spatial and temporal derivatives of λ_i and V_i for all $t \in (0, T]$. Under assumptions 1 and 2, the following convergence bound holds:*

$$\|W_1^n - V_1^n\| + \|W_2^n - V_2^n\| \leq T \exp(C_* T) [O(h^2/\Delta t) + O(\Delta t)] \quad \text{for all } n = 1, 2, \dots, N. \quad (40)$$

Proof. We first bound $\|W_1^n - V_1^n\|$. One has

$$\|W_1^n - V_1^n\| \leq \|W_1^n - \Pi_h V_1^n\| + \|\Pi_h V_1^n - V_1^n\|.$$

We apply Lemma 1 to plug in $V_1^n = V_1^{n-1}(g_1^{n-1})$ and then bound the first term as follows.

$$\begin{aligned} \|W_1^n - \Pi_h V_1^n\| &\leq \|\Pi_h[W_1^{n-1}(\tilde{g}_1^{n-1})] - \Pi_h[V_1^{n-1}(\tilde{g}_1^{n-1})]\| + \|\Pi_h[V_1^{n-1}(\tilde{g}_1^{n-1})] - \Pi_h[V_1^{n-1}(g_1^{n-1})]\| \\ (\|\Pi_h\| = 1) \quad &\leq \|W_1^{n-1}(\tilde{g}_1^{n-1}) - V_1^{n-1}(\tilde{g}_1^{n-1})\| + \|V_1^{n-1}(\tilde{g}_1^{n-1}) - V_1^{n-1}(g_1^{n-1})\| \\ &\leq \|W_1^{n-1} - V_1^{n-1}\| + \|(V_1^{n-1})'\| \|\tilde{g}_1^{n-1} - g_1^{n-1}\| \end{aligned}$$

To bound $\|\tilde{g}_1^{n-1} - g_1^{n-1}\|$, note that for any x , we have

$$\begin{aligned} |\tilde{g}_1^{n-1}(x) - g_1^{n-1}(x)| &= |\mathcal{I}_1^{n-1}(x) - \tilde{\mathcal{Q}}_1^{n-1}(x)| \\ &\leq |\mathcal{I}_1^{n-1}(x) - \mathcal{Q}_{1,R}^{n-1}(x)| + |\mathcal{Q}_{1,R}^{n-1}(x) - \tilde{\mathcal{Q}}_1^{n-1}(x)|. \end{aligned}$$

The first term is the quadrature error due to the rectangle rule and the second term may be bounded in the following way:

$$\begin{aligned} |\mathcal{Q}_{1,R}^{n-1}(x) - \tilde{\mathcal{Q}}_1^{n-1}(x)| &\leq |\mathcal{Q}_{1,R}^{n-1}(x) - \mathcal{Q}_1^{n-1}(x)| + |\mathcal{Q}_1^{n-1}(x) - \tilde{\mathcal{Q}}_1^{n-1}(x)| \\ &= \Delta t |\phi_1(V_1^{n-1}(g_1^{n-1}(x)), V_2^{n-1}(g_1^{n-1}(x))) - \phi_1(V_1^{n-1}(x), V_2^{n-1}(x))| \\ &\quad + \Delta t |\phi_1(V_1^{n-1}(x), V_2^{n-1}(x)) - \phi_1(W_1^{n-1}(x), W_2^{n-1}(x))| \\ (\text{by Lipschitz continuity}) \quad &\leq \Delta t C_{1,\lambda} \{ |V_1^n(g_1^{n-1}(x)) - V_1^{n-1}(x)| + |V_2^n(g_1^{n-1}(x)) - V_2^{n-1}(x)| \\ &\quad + |W_1^{n-1}(x) - V_1^{n-1}(x)| + |W_2^{n-1}(x) - V_2^{n-1}(x)| \} \\ &\leq \Delta t C_{1,\lambda} \{ \|(V_1^{n-1})'\| |g_1^{n-1}(x) - x| + \|(V_2^{n-1})'\| |g_1^{n-1}(x) - x| \\ &\quad + |W_1^{n-1}(x) - V_1^{n-1}(x)| + |W_2^{n-1}(x) - V_2^{n-1}(x)| \} \\ &\leq \Delta t^2 \|\lambda_1\|_T C_{1,\lambda} \{ \|(V_1^{n-1})'\| + \|(V_2^{n-1})'\| \} \\ &\quad + \Delta t C_{1,\lambda} \{ |W_1^{n-1}(x) - V_1^{n-1}(x)| + |W_2^{n-1}(x) - V_2^{n-1}(x)| \}. \end{aligned}$$

With this bound, one has

$$\begin{aligned} \|\tilde{g}_1^{n-1} - g_1^{n-1}\| &\leq \|\mathcal{I}_1^{n-1} - \mathcal{Q}_{1,R}^{n-1}\| + \Delta t C_{1,\lambda} \{ \|W_1^{n-1} - V_1^{n-1}\| + \|W_2^{n-1} - V_2^{n-1}\| \} \\ &\quad + \Delta t^2 \|\lambda_1\|_T C_{1,\lambda} \{ \|(V_1^{n-1})'\| + \|(V_2^{n-1})'\| \}. \end{aligned}$$

With assumption 1, we bound the terms involving the norm of the first derivative of V_i for $i = 1, 2$ and $n = 1 \dots N$.

$$\|(V_i^n)'\| \leq \hat{C} \quad (41)$$

$$\|(V_i^n)'\| C_{i,\lambda} \leq \tilde{C} \quad (42)$$

$$\|(V_i^n)'\| \{ \|(V_1^n)'\| + \|(V_2^n)'\| \} \|\lambda_i\|_T C_{i,\lambda} \leq \bar{C} \quad (43)$$

These constants imply the following bound:

$$\|W_1^n - V_1^n\| \leq (1 + \Delta t \tilde{C}) \|W_1^{n-1} - V_1^{n-1}\| + \Delta t \tilde{C} \|W_2^{n-1} - V_2^{n-1}\| + \|\Pi_h V_1^n - V_1^n\| + \hat{C} \|\mathcal{I}_1^{n-1} - \mathcal{Q}_{1,R}^{n-1}\| + \bar{C} \Delta t^2.$$

The same argument as above provides the bound for the error in the second characteristic variable:

$$\|W_2^n - V_2^n\| \leq (1 + \Delta t \tilde{C}) \|W_2^{n-1} - V_2^{n-1}\| + \Delta t \tilde{C} \|W_1^{n-1} - V_1^{n-1}\| + \|\Pi_h V_2^n - V_2^n\| + \hat{C} \|\mathcal{I}_2^{n-1} - \mathcal{Q}_{2,R}^{n-1}\| + \bar{C} \Delta t^2.$$

Summing the two above inequalities, one obtains:

$$\begin{aligned} \|W_1^n - V_1^n\| + \|W_2^n - V_2^n\| &\leq (1 + 2\Delta t \tilde{C}) \{ \|W_1^{n-1} - V_1^{n-1}\| + \|W_2^{n-1} - V_2^{n-1}\| \} \\ &\quad + \|\Pi_h V_1^n - V_1^n\| + \|\Pi_h V_2^n - V_2^n\| \\ &\quad + \hat{C} \{ \|\mathcal{I}_1^{n-1} - \mathcal{Q}_{1,R}^{n-1}\| + \|\mathcal{I}_2^{n-1} - \mathcal{Q}_{2,R}^{n-1}\| \} \\ &\quad + 2\bar{C} \Delta t^2 \\ &\leq \exp(2\Delta t \tilde{C}) \{ \|W_1^{n-1} - V_1^{n-1}\| + \|W_2^{n-1} - V_2^{n-1}\| \} \\ &\quad + \|\Pi_h V_1^n - V_1^n\| + \|\Pi_h V_2^n - V_2^n\| \\ &\quad + \hat{C} \{ \|\mathcal{I}_1^{n-1} - \mathcal{Q}_{1,R}^{n-1}\| + \|\mathcal{I}_2^{n-1} - \mathcal{Q}_{2,R}^{n-1}\| \} \\ &\quad + 2\bar{C} \Delta t^2. \end{aligned}$$

We apply the same argument to successively bound the terms $\|W_1^j - V_1^j\| + \|W_2^j - V_2^j\|$ and conclude:

$$\begin{aligned} \|W_1^n - V_1^n\| + \|W_2^n - V_2^n\| &\leq \sum_{j=1}^n \exp(2\Delta t \tilde{C})^{n-j} \{ \|\Pi_h V_1^j - V_1^j\| + \|\Pi_h V_2^j - V_2^j\| \} \\ &\quad + \sum_{j=1}^{n-1} \exp(2\Delta t \tilde{C})^{n-1-j} \hat{C} \{ \|\mathcal{I}_1^j - \mathcal{Q}_{1,R}^j\| + \|\mathcal{I}_2^j - \mathcal{Q}_{2,R}^j\| \} \\ &\quad + \sum_{j=1}^n 2\bar{C} \exp(2\Delta t \tilde{C})^{n-j} \Delta t^2 \\ &\leq n \exp(C_* \Delta t)^n \left[\max_{i,j} \{ \|\Pi_h V_i^j - V_i^j\| + \max_{i,j} \|\mathcal{I}_i^j - \mathcal{Q}_{i,R}^j\| + O(\Delta t^2) \} \right] \\ &\leq \frac{T}{\Delta t} \exp(C_* T) \left[\max_{i,j} \|\Pi_h V_i^j - V_i^j\| + \max_{i,j} \|\mathcal{I}_i^j - \mathcal{Q}_{i,R}^j\| + O(\Delta t^2) \right]. \end{aligned}$$

where $C_* > 0$ is a new constant, large enough such that we can take all the prefactors outside the parentheses. The maximum is taken over $i = 1, 2$ and $j = 1, \dots, n$. For the rectangle rule, one can show:

$$\max_j \|\mathcal{I}_i^j - \mathcal{Q}_{i,R}^j\| \leq \frac{\Delta t^2}{2} (\|\lambda_i'\|_T \|\lambda_i\|_T + \|\lambda_i\|_T) \quad (44)$$

For piecewise linear interpolation, we have:

$$\max_j \|\Pi_h V_i^j - V_i^j\| \leq \frac{h^2}{8} \|V_i''\|_T. \quad (45)$$

With these bounds we obtain the result. \square

Remark 4. *Practically we take $h = C\Delta t$ for some constant C , so the error decreases linearly in both Δt and h . Notice that neither the Stability Proposition 2 nor the Convergence Theorem 1 are dependent on the choice for the constant C . In fact, in order to obtain convergence at a linear rate, it is only needed that $h/\Delta t$ is bounded above. In other words, our proposed method is unconditionally stable with no need to satisfy a CFL-type condition.*

5. Numerical Experiments

5.1. Convergence rate and unconditional stability

We compute the convergence rate of our method by comparing our numerical solution to the exact solution

$$A(x, t) = \left(1 + t \exp(-10t) \sin \frac{\pi x}{L}\right)^2 \quad (46)$$

$$u(x, t) = 0 \quad (47)$$

with boundary conditions $A = A_0 = 1 \text{ cm}^2$ on the inlet and outlet. The spatial variable $x \in [0, L]$ for $L = 20 \text{ cm}$. The time variable $t \in [0, T]$ where $T = 1 \text{ sec}$. The characteristic variables V_1 and V_2 are then derived from (11) – (12). Following the test case presented in [31], the parameters are chosen as $\beta = 229674 \text{ dyne/cm}^3$ and $\mu = 0$. Using the standard approach, we derive the source terms for this exact solution and then compute a numerical approximation with NMC. Following Proposition 1, we approximately integrate the right-hand side of (13) using the simplest explicit quadrature rule. See Algorithm 2 for this augmented version of the NMC algorithm.

To highlight the performance of the method beyond the traditional CFL limitation, let us consider the following constant

$$K_{\text{CFL}} := \frac{c_0 \Delta t}{h}, \quad \text{where } c_0^2 = \frac{\beta}{2\rho} A_0^{1/2}. \quad (48)$$

Here c_0 approximates the speed of pressure waves. Explicit methods require K_{CFL} to be bounded (typically less than 1) for stability, but our method requires no such restriction. In this light, we set $K_{\text{CFL}} = 2^n$ to investigate the convergence behavior of the method as n increases. Table 1 displays

Algorithm 2 NMC algorithm augmented to account for source term

- 1: **Input:** $V_1^0, V_2^0 \in C[a, b]$.
 - 2: Initialize $W_1^0 = \Pi_h[V_1^0]$ and $W_2^0 = \Pi_h[V_2^0]$.
 - 3: for $n = 1, 2, \dots, N$
 - 4: $\tilde{g}_1^{n-1}(x) = x - \Delta t \phi_1(W_1^{n-1}(x), W_2^{n-1}(x))$
 - 5: $\tilde{g}_2^{n-1}(x) = x - \Delta t \phi_2(W_1^{n-1}(x), W_2^{n-1}(x))$
 - 6: $W_1^n(x) = \Pi_h[W_1^{n-1}(\tilde{g}_1^{n-1}(x)) + \Delta t \hat{S}_1(W_1^{n-1}(\tilde{g}_1^{n-1}(x)), W_2^{n-1}(\tilde{g}_1^{n-1}(x)))]$
 - 7: $W_2^n(x) = \Pi_h[W_2^{n-1}(\tilde{g}_2^{n-1}(x)) + \Delta t \hat{S}_2(W_1^{n-1}(\tilde{g}_2^{n-1}(x)), W_2^{n-1}(\tilde{g}_2^{n-1}(x)))]$
 - 8: end
-

relative error in the supremum norm (over space and time) and convergence rate for different values of K_{CFL} , and $h = L/2^{3+m}$ and $\Delta t = K_{\text{CFL}}h/c_0$ for $m = 1, \dots, 6$.

m	Rel Error						
	$K_{\text{CFL}} = 1/4$	$K_{\text{CFL}} = 1/2$	$K_{\text{CFL}} = 1$	$K_{\text{CFL}} = 2$	$K_{\text{CFL}} = 4$	$K_{\text{CFL}} = 8$	$K_{\text{CFL}} = 16$
1	1.77×10^{-3}	1.25×10^{-3}	2.73×10^{-3}	5.53×10^{-3}	1.10×10^{-2}	2.07×10^{-2}	7.22×10^{-2}
2	9.80×10^{-4}	6.32×10^{-4}	1.38×10^{-3}	2.77×10^{-3}	5.57×10^{-3}	1.10×10^{-2}	2.08×10^{-2}
3	5.18×10^{-4}	3.19×10^{-4}	6.92×10^{-4}	1.39×10^{-3}	2.78×10^{-3}	5.59×10^{-3}	1.11×10^{-2}
4	2.66×10^{-4}	1.60×10^{-4}	3.47×10^{-4}	6.95×10^{-4}	1.39×10^{-3}	2.78×10^{-3}	5.59×10^{-3}
5	1.35×10^{-4}	8.03×10^{-5}	1.74×10^{-4}	3.48×10^{-4}	6.96×10^{-4}	1.39×10^{-3}	2.78×10^{-3}
6	6.80×10^{-5}	4.02×10^{-5}	8.69×10^{-5}	1.74×10^{-4}	3.48×10^{-4}	6.96×10^{-4}	1.39×10^{-3}
m	Conv Rate						
	$K_{\text{CFL}} = 1/4$	$K_{\text{CFL}} = 1/2$	$K_{\text{CFL}} = 1$	$K_{\text{CFL}} = 2$	$K_{\text{CFL}} = 4$	$K_{\text{CFL}} = 8$	$K_{\text{CFL}} = 16$
2	0.85	0.98	0.99	1.00	0.98	0.91	1.80
3	0.92	0.99	0.99	1.00	1.00	0.98	0.91
4	0.96	0.99	1.00	1.00	1.00	1.01	0.98
5	0.98	1.00	1.00	1.00	1.00	1.00	1.01
6	0.99	1.00	1.00	1.00	1.00	1.00	1.00

Table 1: Relative errors in the supremum norm (over space and time) for the NMC. The asymptotic linear rate of convergence proven in Theorem 1 is observed in these numerical experiments for increasing values of the CFL number K_{CFL} . These experiments confirm the unconditional stability of the NMC.

5.2. Single uniform vessel

In this section, we compare the numerical method of characteristics applied to (13) for approximating (V_1, V_2) to a discontinuous Galerkin (dG) discretization applied to (1) for approximating (A, u) (as described by Sherwin et al. [4]). The computational domain is a single vessel of length 20 cm. The vessel parameters are again derived from the test case presented in [31]; $A_0 = 1 \text{ cm}^2$ and $\beta = 229674 \text{ dyne/cm}^3$. An initial Gaussian pressured pulse in time is prescribed at the left inlet of the vessel with functional form

$$p(t) = \alpha \exp\left((t - \xi)^2/2\sigma^2\right). \quad (49)$$

The parameters $\alpha = 10^2$ or 10^3 dyne/cm^2 , $\xi = 0.015 \text{ s}$, $\sigma = 0.003 \text{ s}$ remain the same for each numerical experiment in this section. Further, we set the viscosity $\mu = 0$ so that we can attribute

any possible diffusion to the numerical method itself. From this pressure pulse, one derives the prescribed area at the inlet from the state equation, and the velocity at the inlet from extrapolating the outgoing characteristic (V_2) to the boundary. This characteristic extrapolation procedure ensures that the equations are approximately satisfied on the inlet boundary.⁴

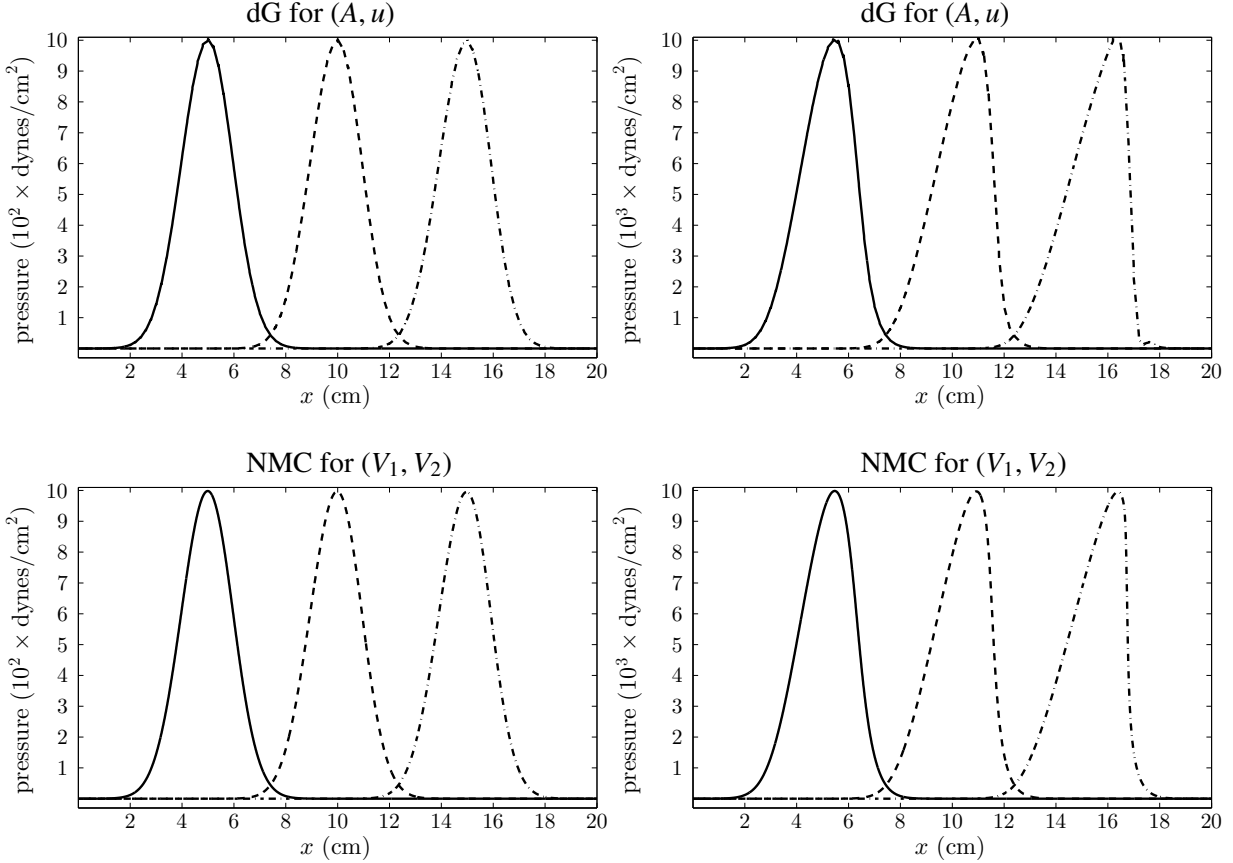


Figure 2: Propagation of Gaussian pressure pulse in a single uniform vessel, simulated with discontinuous Galerkin (top) and numerical method of characteristics (bottom). The dG implementation uses 100 elements with piecewise linear polynomials and $\Delta t = 1 \times 10^{-5}$, while the NMC implementation uses a spatial discretization of 1×10^{-2} and $\Delta t = 1 \times 10^{-4}$. Time increases from the left to right with snapshots taken every 0.03 seconds, i.e. for the solid line, $t = 0.03$, for the dashed line, $t = 0.045$, and for the dotted-dashed line, $t = 0.06$. As expected, the NMC method exhibits some small numerical dissipation, but agrees very well with the dG simulation. For the figures on the right, the amplitude of the wave is an order of magnitude larger than in the figures on the left, leading to rapid shock formation within the computational domain.

As a metric for comparing the approximate solutions obtained from NMC and dG, define the vectors \mathbf{p}_{dG} and \mathbf{p}_{NMC} as the pressures computed from each method with each component corresponding to a pressure value at a point in the NMC grid G_h . Then the relative difference is

⁴Prescribing boundary conditions for these equations is a subtle procedure; we do not dwell on these details in this paper. For more information, see e.g. [4] as well as other works in 1d hemodynamic modeling.

given by

$$\frac{\|\mathbf{p}_{dG} - \mathbf{p}_{NMC}\|_2}{\|\mathbf{p}_{dG}\|_2} \quad (50)$$

where $\|\cdot\|_2$ is the vector two-norm. Figure 2 displays the approximate solutions to both methods for $\alpha = 10^2$ (no shock) and $\alpha = 10^3$ (shock) respectively. Visually, they appear to agree well, modulo some small diffusion in the NMC solution. Table 2 displays the relative difference between the dG and NMC solutions at each of the times $t = 0.03, 0.045$, and 0.06 , and confirms the agreement of the solutions. The two methods agree less well in capturing the shock, but we note that shock formation is not physiological for normal blood flow.

α	$\ \mathbf{p}_{dG} - \mathbf{p}_{NMC}\ _2 / \ \mathbf{p}_{dG}\ _2$		
	$t = 0.03$	$t = 0.045$	$t = 0.06$
10^2	2.77×10^{-3}	3.71×10^{-3}	4.95×10^{-3}
10^3	1.01×10^{-2}	3.03×10^{-2}	8.53×10^{-2}

Table 2: Relative difference in dG and NMC solutions for simulations within a single vessel.

Lastly, Figure 3 displays timing results for MATLAB implementations of each method applied to the simulation of a pressure pulse in a single vessel. For both cases, $\Delta t = 1 \times 10^{-6}$ and the degrees of freedom (*DOF*) for each method is defined as follows. For dG,

$$DOF = \{\text{number of elements}\} \times \{\text{polynomial degree} + 1\}, \quad (51)$$

and for NMC,

$$DOF = \text{number of points in } G_h. \quad (52)$$

We integrate the solution for 20 timesteps (the final time $T = 2 \times 10^{-5}$) on a laptop with a 2.5 GHz Intel Core i5-2520M processor. The value displayed in Figure 3 is wall clock time, averaged over 25 realizations, normalized by T , and then divided by *DOF*. As expected, both methods are asymptotically linear in *DOF*, with NMC several of orders of magnitude faster than dG.

5.3. Vessel network

In this section we demonstrate the utility of the numerical method of characteristics in simulating flow in a network of vessels, each modeled by (1). We set up the arterial network from [9] which contains the 64 largest arteries in the human body (we exclude coronary arteries). This arterial tree is connected using 29 nodes at which we enforce conservation of mass and continuity of total pressure. The purpose of this numerical experiment is only to test the applicability of the proposed NMC to simulate blood flow in a domain other than a single vessel. Therefore, for sake of simplicity, we do not incorporate the influence of organs, capillary beds or the venous network. There is no resistance imposed at the terminal ends of this arterial model where the pressure waves are allowed to leave the terminal vessels without reflection. We do take into account the blood viscosity by retaining the zeroth order (dissipative) term of the governing system (13), and employing the augmented NMC algorithm defined in Section 5.1.

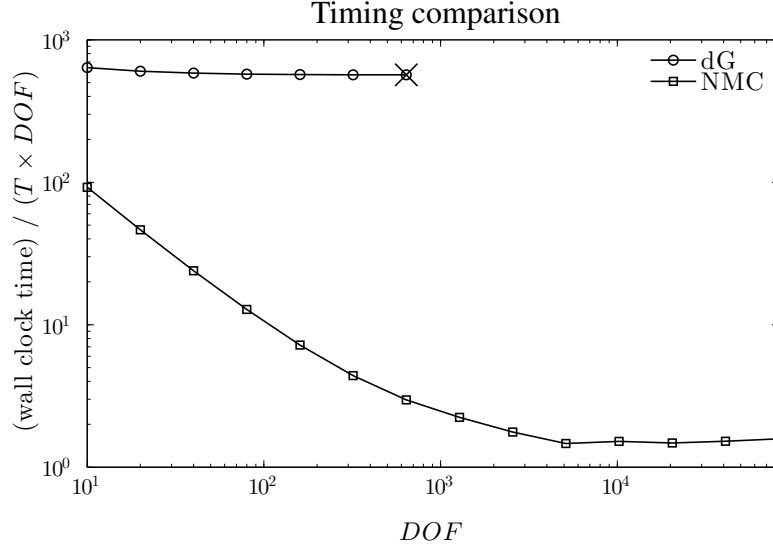


Figure 3: A comparison of the computational time for NMC and dG methods applied to the simulation of a pressure pulse in a single vessel. Both methods asymptotically scale linearly in DOF , with NMC substantially faster than dG. The ‘x’ on the dG curve indicates that for this spatial discretization and beyond, we cannot expect the method to be stable for the chosen timestep.

The length and radius of each arterial segment is obtained from [9]. The elastic coefficient β of each segment is given by

$$\beta = \frac{\delta}{r} \frac{E}{(1 - \sigma^2)r}$$

where $\delta/r = 0.1$ is the ratio of wall thickness δ to unperturbed cross-sectional radius r . The Poisson’s ratio is $\sigma = 0.5$, and E is the Young’s modulus of elasticity. This modulus is determined by the following empirical formula,

$$E = \frac{r}{\delta} \left(6 \times 10^6 e^{-9r/\text{cm}} + 33.7 \times 10^4 \right) \text{ dyne / cm}^2. \quad (53)$$

Figure 4 displays the input pressure profile at the Aortic root and the observed pressure at the left Radial artery. From the given geometry and elastic properties of this arterial tree, we obtain a pressure wave speed c_0 varying within the following range 460 – 1300 cm/sec. The simulation was carried out with a quasi-uniform spatial discretization $h = 0.5$ cm and time step $\Delta t_{\text{NMC}} = 2.5 \times 10^{-3}$ sec which is sufficient to appropriately resolve the pressure variations within one cardiac cycle. As a result, we have a maximum CFL number $K_{\text{CFL}} \approx 6.5$.

On the other hand, the time step needed to satisfy stability for a piecewise linear explicit dG scheme is known to be

$$\Delta t_{\text{dG}} < \frac{h}{3 \max c_0} \approx 1.66 \times 10^{-4}. \quad (54)$$

This implies that Δt_{NMC} is about 15 times larger than Δt_{dG} . The spatial discretization $h = 0.5$ cm leads to about 1600 degrees of freedom (DOF) for the NMC method applied to the entire arterial tree. If we consider both the gain in computational speed per DOF (displayed in Figure 3) and

the larger time step allowed by the unconditional stability of the NMC, then we conclude that the NMC is at least 3 orders of magnitude more efficient than the dG method for these physiological parameters.

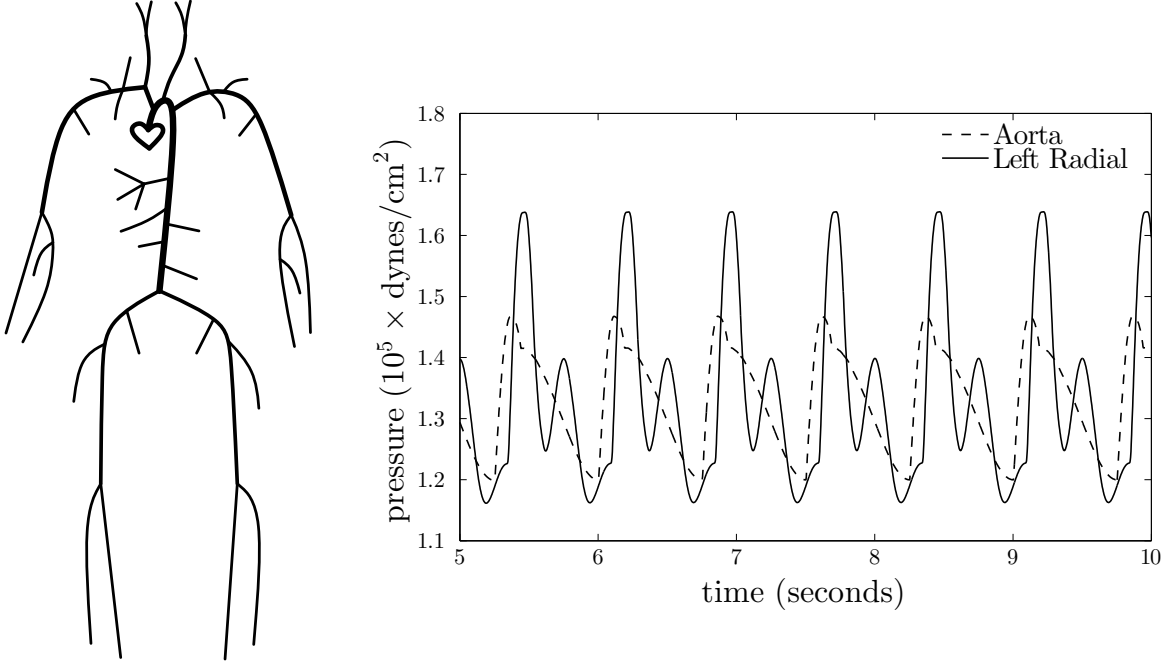


Figure 4: Left: A sketch of the systemic arterial network containing 64 segments and 29 nodes. The geometric and elastic properties of the vessels are provided in Table F.1 of [9]. Right: Pressure waveform (at the aorta and left radial arteries) obtained from the simulation based on the NMC. There is no resistance imposed at the terminal ends.

6. Conclusion

In this work, we focused on the numerical approximation of solutions to a nonlinear, strictly hyperbolic system modeling one-dimensional blood flow. Typical physiological parameters lead to large pressure wave speeds and hence to a restrictive CFL condition for methods using explicit time-stepping for the primitive governing equations. This stringent condition is magnified for computationally intensive methods arising from weak formulations, in simulations of networks of vessels, and for simulations required over multiple cardiac cycles.

To mitigate these challenges, we presented a numerical method of characteristics approach applied to this system. Unconditional stability and convergence of the method was proven. The unconditional stability allows for more rapid simulations beyond the traditional CFL limitation.

To benchmark and test our method, we computed errors and convergence rates from a specified exact solution. Further, solution quality for a propagating Gaussian pressure pulse was compared to an approximation from a discontinuous Galerkin implementation. As expected, numerical diffusion occurs in our method for coarse spatial discretizations, but a marginally more refined discretization yields much better results. Lastly, we applied the method to a network of vessels. From

the timing results for the dG and NMC implementations, and due to the larger time-step allowed for NMC, we conclude that NMC is at least 1000 times more efficient than dG.

Future work will entail clinical applications of vessel network simulations including the influence of organs, capillary beds, and the venous network. These full cardiovascular models, simulated with the numerical method of characteristics, will allow researchers and clinicians to investigate challenging physiological questions from a computational modeling perspective. Furthermore, the efficiency of our approach allows for simulations over a large number of heart cycles on modest computational capabilities. In turn, this opens a door for a much more computationally tractable approach for modeling these phenomena.

7. Acknowledgments

This work was funded in part by NSF grant NSF-DMS 1312391 and by a training fellowship from the Keck Center of the Gulf Coast Consortia, on the Training Program in Biomedical Informatics, National Library of Medicine (NLM) T15LM007093.

References

- [1] S. Čanić, E. H. Kim, Mathematical analysis of the quasilinear effects in a hyperbolic model blood flow through compliant axi-symmetric vessels, *Mathematical Methods in the Applied Sciences* 26 (14) (2003) 1161–1186.
- [2] L. Formaggia, J.-F. Gerbeau, F. Nobile, A. Quarteroni, On the coupling of 3d and 1d Navier–Stokes equations for flow problems in compliant vessels, *Computer Methods in Applied Mechanics and Engineering* 191 (6) (2001) 561–582.
- [3] L. Formaggia, F. Nobile, A. Quarteroni, A one dimensional model for blood flow: application to vascular prosthesis, in: *Mathematical Modeling and Numerical Simulation in Continuum Mechanics*, Springer, 2002, pp. 137–153.
- [4] S. Sherwin, L. Formaggia, J. Peiro, V. Franke, Computational modelling of 1D blood flow with variable mechanical properties and its application to the simulation of wave propagation in the human arterial system, *International Journal for Numerical Methods in Fluids* 43 (6-7) (2003) 673–700.
- [5] P. Blanco, R. Feijóo, S. Urquiza, A unified variational approach for coupling 3d–1d models and its blood flow applications, *Computer Methods in Applied Mechanics and Engineering* 196 (41) (2007) 4391–4410.
- [6] L. Formaggia, F. Nobile, A. Quarteroni, A. Veneziani, Multiscale modelling of the circulatory system: a preliminary analysis, *Computing and Visualization in Science* 2 (2-3) (1999) 75–83.
- [7] P. Blanco, R. Feijóo, A dimensionally-heterogeneous closed-loop model for the cardiovascular system and its applications, *Medical Engineering and Physics* 35 (5) (2013) 652–667.
- [8] E. Marchandise, M. Willemet, V. Lacroix, A numerical hemodynamic tool for predictive vascular surgery, *Medical Engineering and Physics* 31 (1) (2009) 131–144.
- [9] J. P. Mynard, Computer modelling and wave intensity analysis of perinatal cardiovascular function and dysfunction, Ph.D. thesis, The University of Melbourne (2011).
- [10] O. Delestre, P.-Y. Lagrée, A well-balanced finite volume scheme for blood flow simulation, *International Journal for Numerical Methods in Fluids* 72 (2) (2013) 177–205.
- [11] L. Formaggia, D. Lamponi, A. Quarteroni, One-dimensional models for blood flow in arteries, *Journal of Engineering Mathematics* 47 (3-4) (2003) 251–276.
- [12] X. Wang, J.-M. Fullana, P.-Y. Lagre, Verification and comparison of four numerical schemes for a 1d viscoelastic blood flow model, *Computer Methods in Biomechanics and Biomedical Engineering* 0 (0) (2014) 1–22. doi: 10.1080/10255842.2014.948428.
URL <http://dx.doi.org/10.1080/10255842.2014.948428>

- [13] J. Douglas Jr., T. Russell, Numerical methods for convection-dominated diffusion problems based on combining the method of characteristics with finite element or finite difference procedures, *SIAM J. Numer. Anal.* 19 (5) (1982) 871–885.
- [14] Y. Hasbani, E. Livne, M. Bercovier, Finite elements and characteristics applied to advection-diffusion equations, *Computers and Fluids* 11 (2) (1983) 71–83.
- [15] R. E. Ewing, T. F. Russell, M. F. Wheeler, Convergence analysis of an approximation of miscible displacement in porous media by mixed finite elements and a modified method of characteristics, *Comput. Methods Appl. Mech. Engrg.* 47 (1–2) (1984) 73–92.
- [16] T. Russell, Time stepping along characteristics with incomplete iteration for a Galerkin approximation of miscible displacement in porous media, *SIAM J. Numer. Anal.* 22 (5) (1985) 970–1013.
- [17] S. Krishnamachari, L. Hayes, T. F. Russell, A finite element alternating-direction method combined with a modified method of characteristics for convection-diffusion problems, *SIAM J. Numer. Anal.* 26 (6) (1989) 1462–1473.
- [18] E. Suli, A. Ware, A spectral method of characteristics for hyperbolic problems, *SIAM J. Numer. Anal.* 28 (2) (1991) 423–445.
- [19] K. Morton, A. Priestley, E. Suli, Stability of the Lagrange-Galerkin method with non-exact integration, *RAIRO – Model. Math. Anal. Num.* 22 (4) (1988) 625–653.
- [20] O. Pironneau, On the transport-diffusion algorithm and its applications to the Navier-Stokes equations, *Numer. Math.* 38 (1982) 309–332.
- [21] E. Suli, Convergence and nonlinear stability of the Lagrange-Galerkin method for the Navier-Stokes equations, *Numer. Math.* 53 (1988) 459–483.
- [22] Y. Achdou, J.-L. Guermond, Convergence analysis of a finite element projection Lagrange-Galerkin method for the incompressible Navier-Stokes equations, *SIAM J. Numer. Anal.* 37 (3) (2000) 799–826.
- [23] H. Takewaki, T. Yabe, The cubic-interpolated pseudo particle (CIP) method : application to nonlinear and multi-dimensional hyperbolic equations, *J. Comput. Phys.* 70 (1987) 355–372.
- [24] M. Ida, T. Yabe, Implicit CIP (cubic-interpolated propagation) method in one-dimension, *Computer Phys. Commun.* 92 (1995) 21–26.
- [25] R. Tanaka, T. Nakamura, T. Yabe, Constructing exactly conservative scheme in a non-conservative form, *Computer Phys. Commun.* 126 (2000) 232–243.
- [26] S. Yoon, T. Yabe, The unified simulation for incompressible and compressible flow by the predictor-corrector scheme based on the CIP method, *Computer Phys. Commun.* 119 (1999) 149–158.
- [27] V. Melicher, V. Gajdošík, A numerical solution of a one-dimensional blood flow model–moving grid approach, *Journal of Computational and Applied Mathematics* 215 (2) (2008) 512–520.
- [28] I. Korade, Z. Virag, M. Šavar, Numerical simulation of one-dimensional flow in elastic and viscoelastic branching tube, in: 11th. World Congress on Computational Mechanics (WCCM XI), 2014.
- [29] G. Bárdossy, G. Halász, Modeling blood flow in the arterial system, *Periodica Polytechnica : Mechanical Engineering* 55 (1) (2012) 49–55.
- [30] L. C. Evans, *Partial Differential Equations*, 2nd Edition, Providence, Rhode Land: American Mathematical Society, 2010.
- [31] J. Mynard, P. Nithiarasu, A 1D arterial blood flow model incorporating ventricular pressure, aortic valve and regional coronary flow using the locally conservative Galerkin (LCG) method, *Communications in Numerical Methods in Engineering* 24 (5) (2008) 367–417.